The effects of strain and surface roughness scattering on the quasi-ballistic characteristics of a Ge nanowire p-channel field-effect transistor*

Qin Jie-Yu(秦洁宇)[a)b)], Du Gang(杜 刚)[b)], and Liu Xiao-Yan(刘晓彦)[b)†]

[a)] *Shenzhen Graduate School, Peking University, Shenzhen* 518055, *China*
[b)] *Institute of Microelectronics, Peking University, Beijing* 100871, *China*

(Received 4 March 2013; revised manuscript received 11 April 2013)

The effects of strain and surface roughness scattering on the quasi-ballistic hole transport in a strained gate-all-around germanium nanowire p-channel field-effect transistor (pFET) are investigated in this work. The valence subbands are shifted up and warped more parabolically by the influence of HfO_2 due to the lattice mismatch. However, the boundary force only shifts the subbands downwards and has little effect on the reshaping of bands. Strain induced by HfO_2 increases both the hole mobility and ON-current (I_{ON}), but has little effect on the hole mobility. The I_{ON} is degraded by the surface roughness scattering in both strained and unstrained devices.

Keywords: nanowire, strain, surface roughness scattering, quasi-ballistic

PACS: 71.20.–b, 81.40.Jj, 03.65.Nk, 73.23.Ad **DOI:** 10.1088/1674-1056/22/10/107104

1. Introduction

With the down-scaling of the complementary metal–oxide–semiconductor (CMOS) devices, some kinds of non-planar device architectures (such as Tri-Gate fin field-effect transistors (FinFETs), Ω-Gate FinFETs, and gate-all-around (GAA) metal–oxide–semiconductor field-effect transistors (MOSFETs))[1] are investigated to continue the downscaling of MOSFETs. Germanium is also considered as an alternative channel material due to its higher intrinsic carrier mobility than silicon.[2] Attention has been paid to the GAA Ge nanowire (NW) MOSFET as one of the potential candidates to further the technology roadmap: excellent suppression of the short channel effects (SCEs), high achievement of sub-threshold swing (SS) value and ON-current (I_{ON}).[3]

High permittivity (or high-k) dielectrics (such as HfO_2) and metal gates[4,5] are widely used to achieve the ultimate equivalent oxide thickness (EOT) and boost the performance of devices. Experimental work indicates that the process and material-induced stress can influence the performance of an NW device.[6] Carrier mobility is strongly dependent on strain and surface conditions,[7,8] which will further affect the characteristics of the strained device. However, there are few reports on the quasi-ballistic characteristics of strained Ge NW FETs. Therefore, the effects of different stressors and scattering mechanisms on the performances of Ge NW FETs still need further investigation.

We have presented the strain influence on the valence band of a silicon nanowire in Ref. [9]. In the present work, we calculate the strain tensor component distributions in the GAA Ge NW pFETs induced by high-k dielectric (HfO_2) and boundary force (300 MPa). The influence of valence band structure variation on strain is also studied. The effects of strain-induced and surface-roughness-scattering-influenced transport on the quasi-ballistic characteristics of Ge nanowire pFETs are presented. The results are important to optimize and develop the model for Ge NW FETs.

2. Simulation method and device structure

The device structure and corresponding parameters of the simulated GAA Ge NW are shown in Fig. 1. The Ge NW is cylindrical in shape, and its cross section in the x–y plane is circlular. The radius of the cylinder Ge NW (R_{Ge}) is 4 nm, and the thickness of the high-k dielectric (HfO_2) (T_{HfO2}) is 2 nm. The axial direction of the Ge NW is (110), which is the same as the transport direction of carriers from the source to the drain (the z axis). The continuum elastic model[10,11] and the finite element method[12,13] are used to calculate the lattice-mismatch-induced and boundary-force-induced strains in the Ge NW. The nanowires are assumed to be infinite in the z direction.[14] For convenience, the basis vectors of the coordinate system in the (110) Ge NW are selected as

$$x = \frac{1}{2}\begin{pmatrix} -1 \\ 1 \\ \sqrt{2} \end{pmatrix}, \quad y = \frac{1}{2}\begin{pmatrix} -1 \\ 1 \\ -\sqrt{2} \end{pmatrix}, \quad z = \frac{1}{\sqrt{2}}\begin{pmatrix} 1 \\ 1 \\ 0 \end{pmatrix}.$$

The 6×6 $\boldsymbol{k} \cdot \boldsymbol{p}$ method[15,16] is used to calculate the valence band, in which the light holes, the heavy holes, and the spilt-off bands are included. The strain is also considered as a

*Project supported by the National Key Basic Research Program, China (Grant Nos. 2011CBA00604 and 2009ZX02305-003).
†Corresponding author. E-mail: xyliu@ime.pku.edu.cn
© 2013 Chinese Physical Society and IOP Publishing Ltd

perturbation Hamiltonian. This model works well in predicting the valence band structure with (or without) the strain effects. The Kubo–Greenwood formula is employed to compute the hole mobility limited by acoustic phonon scattering (ac), optical phonon scattering (op), and surface roughness scattering (sr).[17–19] The surface roughness scattering rate is determined by the roughness of the Ge/HfO_2 interface, which is characterized by the correlation length L and the average step-height Δ.[17,18]

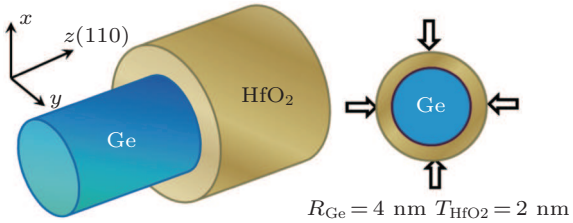


Fig. 1. (color online) The Ge nanowire structure.

A quasi-ballistic model based on backscattering is used to evaluate the I–V characteristics of the Ge NW pFETs. We use McKelvey's flux method[20] to illustrate the drain current and decompose it into the positive and negative directed fluxes. The positively directed flux J^+ originates from the thermal emission from the source. Owning to the presence of scattering, the negatively directed flux J^- is comprised of two components. One component (rJ^+) is due to the backscattering of the positively directed flux. Here, r is the backscattering coefficient and expressed as[21–24]

$$r = \frac{l}{l+\lambda_0} \quad \text{with} \quad \lambda_0 = \frac{kT}{q}\cdot\frac{2\mu}{v_T}, \quad \text{and} \quad v_T = \sqrt{\frac{2kT}{\pi m^*}}, \tag{1}$$

where l is the critical length which is the gate length in the linear region and the width of the "kT-layer" in the saturated region; λ_0 is the mean-free-path related to the carrier mobility; v_T is the unidirectional thermal velocity of the carrier injected from the source side. As a result, the effect of the surface roughness scattering can be included in r.

The other component of J^- is the flux injected from the drain which transmits to the source and is written as rJ_b^-. Here, the subscript b denotes the negatively directed flux under ballistic condition.[21] Adding the two components, the negatively directed flux is expressed as

$$J^- = rJ^+ + (1-r)J_b^-. \tag{2}$$

And the total drain current can be evaluated from

$$J = J^+ - J^-. \tag{3}$$

Equations (1)–(3) summarize the quasi-ballistic model based on the scattering theory. Thus, we are able to evaluate the effects of strain and surface roughness scattering on the quasi-ballistic characteristics of the Ge NW pFETs.

3. Results and discussion

3.1. Strain tensor component distribution

Figure 2 shows the slice strain tensor component distributions along the x axis in the Ge NW with 2-nm HfO_2 gate dielectric and the same Ge NW under 300-MPa boundary force. As shown in Figs. 2(a) and 2(b), compressive ε_{xx} and tensile ε_{yy} are observed in the strained Ge NW. The boundary force increases the compressive ε_{xx} and reduces the tensile ε_{yy} in the device with HfO_2. The shear strain ε_{xy} is very small in both devices. The smaller lattice constant of HfO_2 brings compressive ε_{zz} (-0.0718) in germanium. However, the boundary force applied to the HfO_2 stretches the nanowire along the z axis and degrades the compressive strain ε_{zz} (-0.0705) as shown in Fig. 2(c).

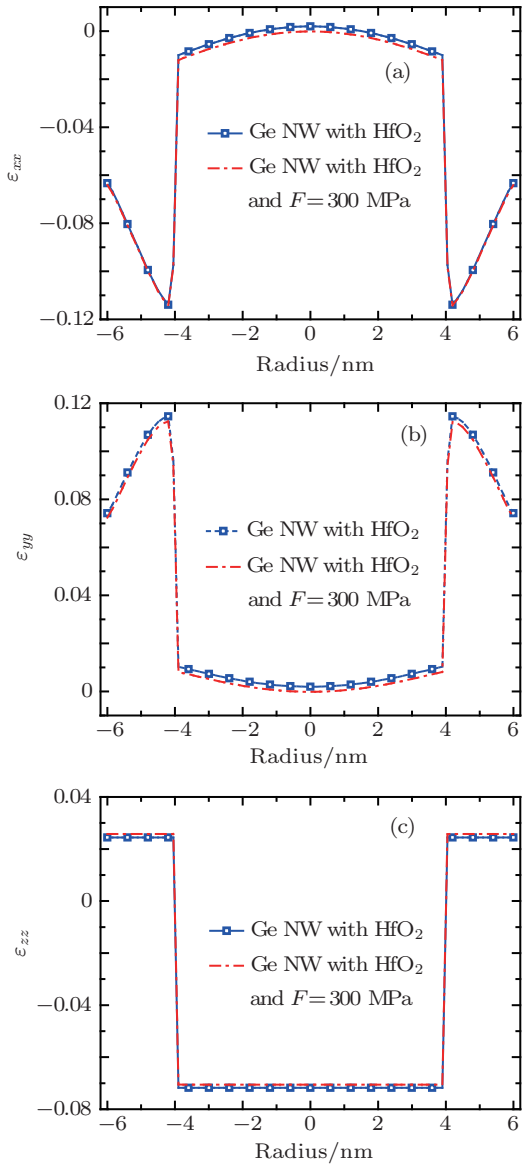


Fig. 2. (color online) Distributions of strain tensor components of (a) ε_{xx}, (b) ε_{yy}, and (c) ε_{zz} along the x axis.

3.2. Valence band structure

The valence band dispersions of the Ge NWs under no strain, lattice-mismatch-induced strain (with HfO_2), and boundary-force-induced strain are respectively plotted in Figs. 3(a), 3(b), and 3(c) each as a function of wave vector k_z. The energy maximum of the unstrained Ge NW is -77.6 meV. The valence subband in the Ge NW with HfO_2 is warped and shifted up, and the energy maximum is 226.4 meV. As shown in Fig. 3(c), the top energy of the Ge NW with both HfO_2 and boundary force is 199.0 meV, which is 27.4 meV lower than that of the device with HfO_2 only. Compared with HfO_2, the boundary force has little effect on the reshaping of the valence subband.

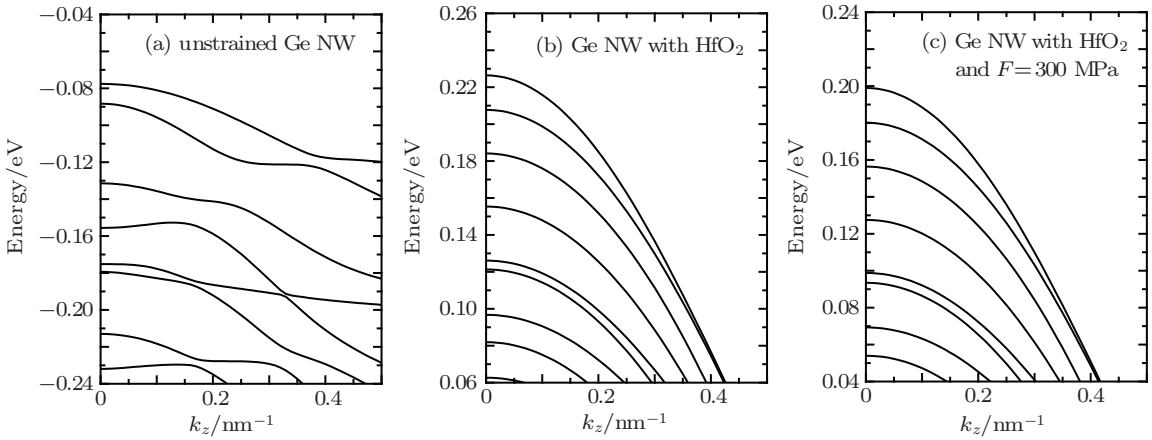


Fig. 3. Valence band structures of different (110) Ge NWs: (a) pure Ge NW, (b) Ge NW with HfO_2, and (c) Ge NW with HfO_2 and 300 MPa boundary force.

Figure 4 shows the values of hole effective mass of the top five subbands in different Ge NWs. Compared with the bands in the unstrained Ge NW, the warped bands in the strained devices result in a light hole effective mass. The effective mass of the first subband in the unstrained Ge NW is $0.111m_0$. However, the effective mass of the Ge NW with HfO_2 is $0.036m_0$, which is only 32% of the former one. The light effective mass is favorable for the increment of the hole mobility. The effective mass in the Ge NW with both HfO_2 and boundary force is almost identical with that of the device with HfO_2 only. This can be understood from Figs. 2(b) and 2(c), and the small band-warping-difference results in little effective-mass-variation.

3.3. Hole mobility

Figure 5 shows the values of hole mobility in strained and unstrained Ge NWs with different scattering mechanisms under different effective electric fields. The hole mobility degenerates with the increase of effective electric field, and increases in the strained device. The unapparent difference in hole effective mass induced by boundary force also leads to little mobility variation. At low effective electric field, the surface roughness scattering has little effect on hole mobility.[11] In the unstrained Ge NW, the hole mobility is about 430 $cm^2 \cdot V^{-1} \cdot s^{-1}$, when the effective electric field is 0.5 MV/cm. However, the hole mobility of the strained Ge NW is about 780 $cm^2 \cdot V^{-1} \cdot s^{-1}$, which exhibits 1.81 times

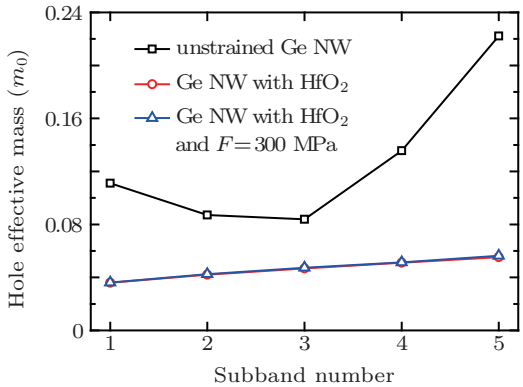


Fig. 4. (color online) Values of effective hole mass of the top five subbands in different Ge NWs. The –o– curve and –△– curve are superposed on each other.

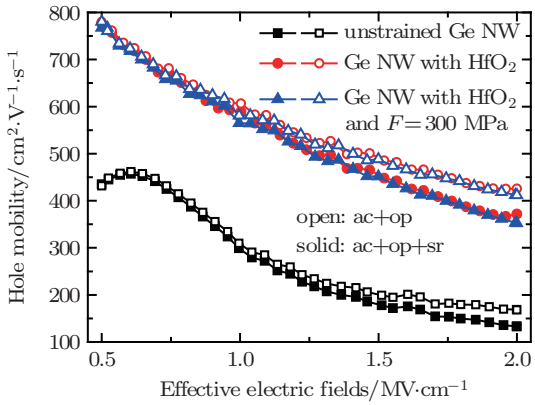


Fig. 5. (color online) Values of effective hole mobility in different Ge NWs with different scattering mechanisms.

mobility gain over the unstrained one and coincides with the experimental result in Ref. [25]. It can be understood by the degraded hole effective mass as shown in Fig. 4. In the case of high effective electric field, the mobility is degraded by the surface roughness scattering. It is because the surface roughness scattering increases with the effective electric field increasing.[17,19]

3.4. Quasi-ballistic characteristics

Figure 6 shows the I_{DS}–V_{GS} characteristics of the Ge NW with HfO_2 under different scattering mechanisms, respectively. The drain current is degraded by the surface-roughness-limited mobility, which results in a smaller mean-free-path and a higher backscattering coefficient.[16] Moreover, larger degradation is observed at higher gate bias. This can be illustrated by Fig. 4, the surface roughness scattering leads to larger mobility degradation at higher $|V_{GS}|$ and increases the backscattering coefficient.

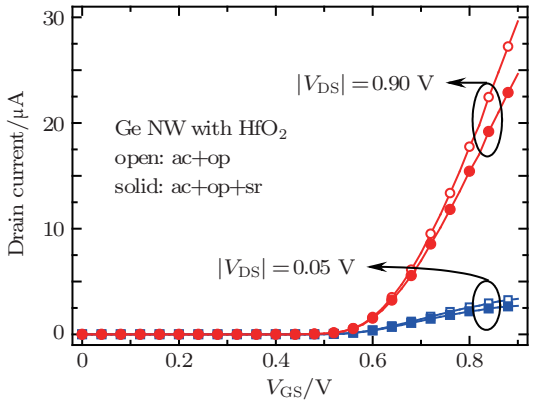


Fig. 6. (color online) The I_{DS}–V_{GS} characteristics of Ge NW pFETs with HfO_2.

Table 1. Values of ON-current (I_{ON}) of different Ge NW pFETs with different scattering mechanisms and stressors. ($|V_{GS}| = |V_{DS}| = 0.90$ V and I_{ON} is in μA).

Scattering mechanism	Stressor		
	Unstrained	HfO_2	HfO_2 + force
ac+op	17.9	29.6	25.9
ac+op+sr	13.7	24.6	21.8

Table 1 summarizes the values of the ON-current (I_{ON}) of different Ge NW pFETs with different scattering mechanisms and stressors. For the unstrained Ge NW pFETs, the I_{ON} affected by the phonon-limited mobility is 17.9 μA. The I_{ON} of the device with HFO_2 is 29.6 μA, which is 65.4% higher than the former one. Larger hole mobility leads to smaller backscattering coefficient and thus larger I_{ON}. Compared with the value of I_{ON} in the device with HfO_2 only, the I_{ON} is degraded by the boundary force. It is because the less up-shifted valence band (Fig. 3(c)) results in less carrier density. The values of I_{ON} of the unstrained and strained device are both degraded by the surface-roughness-limited mobility. The I_{ON} decrement of the unstrained device is 23.5%. The current degradation in the Ge NW with HfO_2 only is 16.9%, and that of the device with both HfO_2 and boundary force is 15.8%. It can be explained by Fig. 5 that the effective hole mobility is degraded by the surface roughness scattering at high gate bias.

Figure 7 shows the backscattering coefficients of the devices with HfO_2 each as a function of gate length under different drain bias. The surface-roughness-limited mobility gives rise to higher backscattering coefficient. The backscattering coefficient increases with gate length increasing and drain bias decreasing.

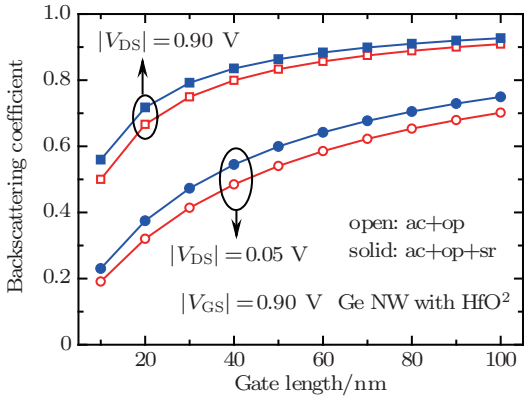


Fig. 7. (color online) Backscattering coefficients of Ge NW pFETs with HfO_2.

4. Conclusions

The effects of phonon-limited hole mobility and surface-roughness-limited hole mobility on the performance of a strained Ge NW pFET are investigated in this work. The surface roughness scattering gives rise to higher backscattering coefficient and results in 16.9% ON-current decrement in the Ge NW pFET with HfO_2 only. The boundary force also reduces the current, and the degradation due to surface roughness scattering is 15.8%. The backscattering coefficient increases with increasing gate length and lower drain bias.

References

[1] Kuhn K J 2012 *IEEE Trans. Electron Dev.* **59** 1813
[2] Lee M L, Leitz C W, Cheng Z, Pitera A J, Langdo T, Currie M T, Taraschi G, Fitzgerald E A and Antoniadis D A 2005 *Appl. Phys. Lett.* **79** 3344
[3] Wang D W, Wang Q, Javey A, Tu R, Dai H J, Kim H, McIntyre P C, Krishnamohan T and Saraswat K C 2003 *Appl. Phys. Lett.* **83** 2432
[4] Radosavljevic M, Dewey G, Basu D, Boardman J, Chu-Kung B, Fastenau J M, Kabehie S, Kavalieros J, Le V, Liu W K, Lubyshev D, Metz M, Millard K, Mukherjee N, Pan L, Pillarisetty R, Rachmady W, Shah U, Then H W and Chau R 2011 *International Electron Devices Meeting*, December 5–7, 2011, Washington DC, USA, p. 33.1.1
[5] Yoshida N, Fu X, Xu K, Lei Y, Yang H, Sun S, Chen H, Darlak A, Donohoe R, Lazik C, Jakkaraju R, Noori A, Hung S, Peidous I, Chang C and Brand A 2012 *Symposium on VLSI Technology and Circuits*, June 12–15, 2012, Honolulu, Hawaii, USA, p. 81
[6] Wang D, Wang Q, Javey A, Tu R, Dai H, Kim H, McIntyre P C, Krishnamohan T and Saraswat K C 2003 *Appl. Phys. Lett.* **83** 2432

[7] Xu H, Liu X, Du G, Fan C, Jin R, Han R and Kang J 2011 *IEEE Trans. Nanotechnol.* **10** 1126
[8] Poli S, Pala M G, Poiroux T, Deleonibus S and Baccarani G 2008 *IEEE Trans. Electron Dev.* **55** 2968
[9] Xu H H, Liu X Y, He Y H, Fan C, Du G, Sun A D, Han R Q and Kang J F 2010 *Chin. Phys. B* **19** 014601
[10] Sondergaard N, He Y, Fan C, Han R Q, Guhr T and Xu H Q 2009 *J. Vac. Sci. Technol. B* **27** 827
[11] Liu Y M, Yu Z Y and Ren X M 2009 *Chin. Phys. B* **18** 16
[12] Zhou W M, Wang, C Y, Chen, Y H and Wang Z G 2006 *Chin. Phys.* **15** 1315
[13] Yu Y T, Yuan W Z, Qiao D Y and Liang Q 2007 *Acta Phys. Sin.* **56** 5691 (in Chinese)
[14] He Y H, Zhao Y N, Fan C. Liu X Y and Han R Q 2009 *Front. Electr. Electron. Eng. China* **4** 342
[15] Kane E O 1956 *J. Phys. Chem. Solids* **1** 82
[16] Bahder T 1990 *Phys. Rev. B* **41** 11992
[17] Fischetti M V, Ren Z, Solomon P M, Yang M and Rim K 2003 *J. Appl. Phys.* **94** 1079
[18] Pham A T, Jungemann C, Nguyen C D and Meinerzhagen B 2006 *Mater. Sci. Eng. B* **135** 224
[19] Zhang Y, Fischetti M V, Soree B and O'Regan T 2010 *J. Appl. Phys.* **108** 123713
[20] McKelvey J P, Longini R L and Brody T P 1961 *Phys. Rev.* **123** 51
[21] Rahman A and Lundstrom M S 2002 *IEEE Trans. Electron Dev.* **49** 481
[22] Lundstrom M 2001 *IEEE Electron Dev. Lett.* **22** 293
[23] Lundstrom M and Ren Z B 2002 *IEEE Trans. Electron Dev.* **49** 133
[24] Lundstrom M 1997 *IEEE Electron Dev. Lett.* **18** 361
[25] Ikeda K, Ono M, Kosemura D, Usuda K, Oda M, Kamimuta Y, Irisawa T, Moriyama Y, Ogura A and Tezuka T 2012 *Symposium on VLSI Technology and Circuits*, June 12–15, 2012, Honolulu, Hawaii, USA, p. 165